

1,2,5,6-Naphthalenediimide Based Donor–Acceptor Copolymers Designed from Isomer Chemistry for Organic Semiconducting Materials

Zheng Zhao,[†] Fengjiao Zhang,[‡] Xu Zhang,[§] Xiaodi Yang,[§] Hongxiang Li,[†] Xike Gao,^{*,†} Chong-an Di,^{*,‡} and Daoben Zhu^{†,‡}

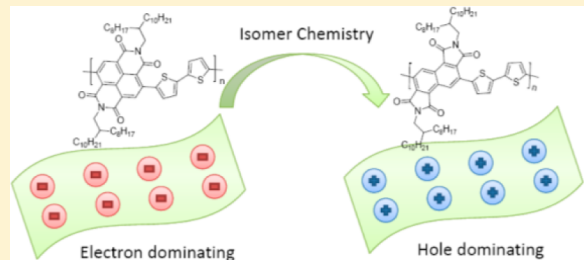
[†]Laboratory of Materials Science, Shanghai Institute of Organic Chemistry, Chinese Academy of Sciences, 345 Lingling Road, Shanghai 200032, China

[‡]Beijing National Laboratory for Molecular Sciences, Key Laboratory of Organic Solids, Institute of Chemistry, Chinese Academy of Sciences, Beijing 100190, China

[§]Laboratory of Advanced Materials, Fudan University, Shanghai 200433, China

Supporting Information

ABSTRACT: Two new donor–acceptor (D–A) copolymers based on 1,2,5,6-naphthalenediimides (iso-NDI) and thiophene units, iso-P(NDI2OD-T2) and iso-P(NDI2OD-TT), were designed from isomer chemistry and compared with the reported isomeric polymers P(NDI2OD-T2) and P(NDI2DT-TT) to investigate the influence of isomeric structure on their optoelectronic properties. DFT calculations reveal that iso-P(NDI2OD-T2) and iso-P(NDI2OD-TT) have higher HOMO and LUMO energies and better backbone planarity relative to their isomeric polymers. Iso-P(NDI2OD-T2) and iso-P(NDI2OD-TT) were synthesized by the Stille coupling polymerization and characterized by elemental analysis, ¹H NMR, GPC, UV–vis absorption, cyclic voltammetry, TGA, DSC, and organic thin film transistors (OTFTs). It was found that iso-P(NDI2OD-T2) and iso-P(NDI2OD-TT) had higher LUMO energies and broader band gaps than their isomeric ones and showed hole-dominated charge transport behavior, which is quite different from the electron-dominated charge transport feature of P(NDI2OD-T2) and P(NDI2DT-TT). In spite of the amorphous-like thin-film features, iso-P(NDI2OD-T2) exhibited high hole mobility of up to $0.3 \text{ cm}^2 \text{ V}^{-1} \text{ s}^{-1}$, and iso-P(NDI2OD-TT) showed ambipolar property with hole and electron mobility of up to 0.02 and $4 \times 10^{-3} \text{ cm}^2 \text{ V}^{-1} \text{ s}^{-1}$, respectively.



INTRODUCTION

Organic semiconducting materials have attracted more and more attention for their applications in low-cost, large-area, and flexible electronic devices.¹ In comparison with small molecular semiconductors, π -conjugated polymeric materials usually have better film-forming ability, solution processability, and mechanical properties,² which are highly important for fabricating thin film devices, especially for the integrated ones.

Up to now, several molecular design strategies have been used for obtaining high performance polymeric semiconductors.³ One strategy is the synthesis of regioregular polymers, such as the regioregular poly(3-hexylthiophene) (rr-P3HT). rr-P3HT has highly ordered architecture and strong interchain π – π interactions, leading to its high hole mobility of 0.1 – $0.3 \text{ cm}^2 \text{ V}^{-1} \text{ s}^{-1}$ for organic thin film transistors (OTFTs).⁴ A second strategy is the incorporation of fused heteroarenes into the conjugated polymer backbones. This approach could result in rigid and planar polymeric backbones, thereby enhancing effective π conjugation and facilitating intra- and intermolecular charge carrier hopping and transporting.⁵ The third approach is the synthesis of alternating donor (D)–acceptor (A) polymers.

The construction of π -conjugated D–A polymers is the most popular strategy to design new high performance semiconductors, especially for the low band gap ones,^{6–9} which could not only form strong interchain interactions that favor charge transport⁷ but also fine-tune the polymers' electronic structures, affording new polymers with desired optoelectronic properties.⁸

The D–A polymers based on rylene diimides are among the best organic semiconductors.^{10–13} There are several virtues for rylene diimides: (1) most of these diimide derivatives own high electron affinity as well as excellent chemical, thermal, and photochemical stability;¹⁴ (2) the bromination of the aromatic core is easy to implement, enabling the modification of aromatic core for diverse semiconducting materials;¹⁴ (3) proper N-substituted groups at the nitrogen atom of the imide group can not only guarantee high solubility for low-cost device fabrication but also achieve efficient molecular packing for high

Received: July 4, 2013

Revised: August 26, 2013

Published: September 17, 2013



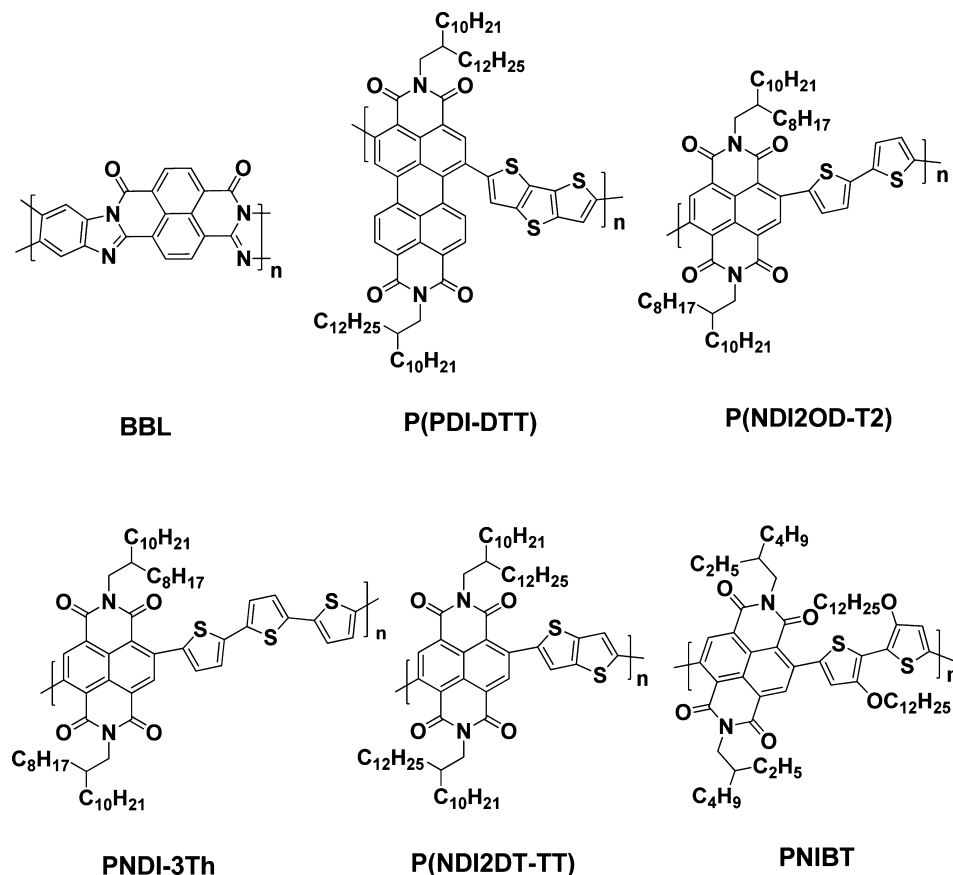


Figure 1. Chemical structures of the representative imide based polymeric semiconductors.

device performance.¹⁵ All of these characteristics make rylene diimides ideal building blocks for constructing D–A polymers.

Perylenediimides (PDIs) and naphthalenediimides (NDIs) are among the best of n-type organic semiconductors.^{11–19} Poly(benzobisimidazobenzophenanthroline) (BBL) (Figure 1), a ladder-type polymer with imide-like structure, exhibits high electron mobility of up to $0.1 \text{ cm}^2 \text{ V}^{-1} \text{s}^{-1}$ and long-term air stability.¹⁶ In 2007, Zhan and co-workers reported a PDI based D–A polymer P(PDI-DTT) (Figure 1) and applied it as active layer for n-channel OTFTs and acceptor for all polymer OPVs,^{11a} which inspired the research of aromatic diimides based D–A polymers.^{10–13} A breakthrough in n-channel polymers for OTFTs occurred with the development of a D–A polymer P(NDI2OD-T2) (Figure 1) by Facchetti and co-workers.¹² Top-gate bottom-contact OTFTs based on P(NDI2OD-T2) display high electron mobility of up to $0.85 \text{ cm}^2 \text{ V}^{-1} \text{s}^{-1}$.^{12a} By varying the number of thiophene units, Luscombe et al. reported a series of NDI-oligothiophene based polymers (PNDI-*n*Th), of which PNNDI-3Th (Figure 1) based bottom-gate top-contact OTFTs exhibited a maximum electron mobility of $0.076 \text{ cm}^2 \text{ V}^{-1} \text{s}^{-1}$.¹³ Jenekhe and Watson et al. reported a series of NDI based polymers containing different donor moieties such as P(NDI2DT-TT) and PNIBT (Figure 1),¹⁷ of which the PNIBT based ambipolar OTFTs and CMOS-like inverters showed excellent performance.^{17a} In addition, Jenekhe et al. reported a series of thiophene-NDI based D–A oligomers (NDI-*n*T); ambipolar charge transport behaviors were observed for these compounds, and bulk heterojunction OPV devices using one of these n-type oligomers as organic acceptor showed a power conversion efficiency (PCE) of up to 1.5% with a high open circuit voltage

of up to 0.82 V .¹⁸ This provides a guide for designing new organic acceptors for OPVs. In addition, new class of aromatic diimide based materials have also been designed and synthesized, some of which displayed excellent device performance.^{15,19,20} All these exciting achievements demonstrate the promising avenue for new rylene diimide based polymers.

Isomeric structures are common in organic π -conjugated materials, especially in organic heteroarenes²¹ and polycyclic aromatic hydrocarbons.²² These isomeric phenomena usually stem from the different positions of heteroatoms/functional groups or the combination styles of molecular moieties. As the study on structure–property relationship, it is highly desired to investigate the influence of isomeric structure on performance of organic electronic materials.^{21–23} It has been shown that under an oxygen atmosphere picene had better chemical stability and device performance than its isomer pentacene.^{22a} Takimiya et al. investigated the influence of isomeric chemistry on the property and performance of naphthodithiophene based polymers and found that isomeric structure had obvious influence on material's electronic structure, physical property, and FET performance.^{23a} The results demonstrate that both molecular shape and molecular electronic structure are important factors for designing new semiconducting materials.^{23a} A series of polymers containing different benzodithiophene isomers and alkylated dithiophenes were synthesized by Müllen and co-workers to investigate the influence of backbone curvature on property and performance of these polymers.^{23b} It turns out that the increased degree of curvature improves the solubility but decreases the orders in thin film, and polymers with intermediate degree of curvature yield the highest charge carrier mobility.^{23b}

1,4,5,8-NDI derivatives have been widely used in supramolecular chemistry, chemical/biological sensors, artificial photosystems, anion transport, and organic semiconducting devices.^{12–20,24} However, up to now, the isomeric 1,2,5,6-NDI derivatives (iso-NDI) and their based materials have been rarely studied.^{25,26} Figure 2 gives the molecular structures,

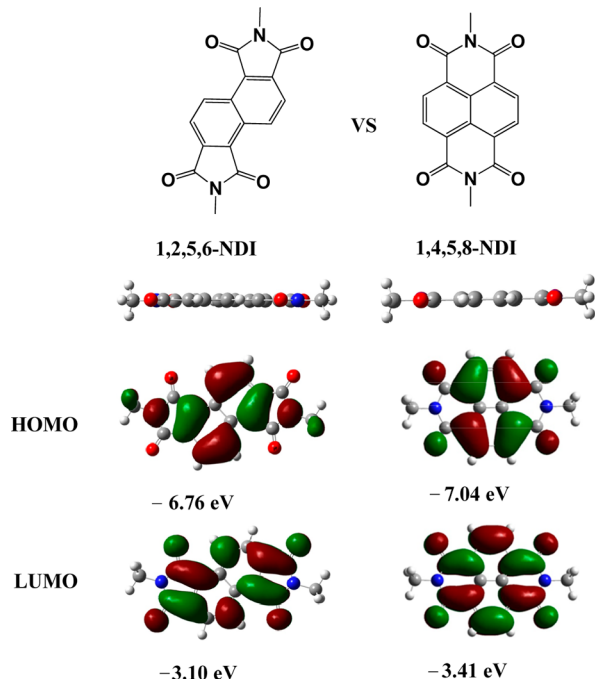


Figure 2. Molecular structures, optimized geometries, frontier orbital wave functions, and energies of 1,2,5,6-NDI and 1,4,5,8-NDI obtained by DFT calculations.

geometries, and frontier orbitals of 1,2,5,6-NDI and 1,4,5,8-NDI estimated by density functional theory (DFT) calculations. Both the angular-shaped 1,2,5,6-NDI and linear 1,4,5,8-NDI show rigid and coplanar π -conjugated backbones. These two isomeric units share the similar electron density distribution of molecular orbital, where the largest coefficients in the HOMO orbital are located on the central naphthalene core, and the coefficients in the LUMO orbital are positioned over the long axis of the molecular backbone. The HOMO and LUMO energies of 1,2,5,6-NDI (-6.76 and -3.10 eV) are higher than those of 1,4,5,8-NDI (-7.04 and -3.41 eV) with the deviation of about 0.3 eV. The different HOMO/LUMO energies of 1,2,5,6-NDI from those of 1,4,5,8-NDI make 1,2,5,6-NDI derivatives promising building blocks for fine-tuning the electronic structures and optoelectronic properties of their based D-A copolymers. More importantly, DFT calculations using thiophene as donor unit (Figure S1) indicate that 1,2,5,6-NDI based D-A polymers may have more coplanar backbones than those of 1,4,5,8-NDI based polymers and therefore will favor charge transport. The more coplanar polymeric backbones might be explained by the smaller steric hindrance between the five-membered imide ring and its adjacent aryl moiety on the naphthalene core.

Herein, we choose 2,2'-bithiophene (T2) and thieno[3,2-b]thiophene (TT) as donor moieties and 1,2,5,6-NDI as acceptor unit to synthesize copolymers iso-P(NDI2OD-T2) and iso-P(NDI2OD-TT) (Figure 3), which can be regarded as the isomeric polymers of the reported P(NDI2OD-T2)¹² and

P(NDI2DT-TT).^{17b} Thermal, optical, and electrochemical properties of iso-P(NDI2OD-T2) and iso-P(NDI2DT-TT) were investigated, and the comparisons between iso-P(NDI2OD-T2)/iso-P(NDI2OD-TT) and P(NDI2OD-T2)/P(NDI2DT-TT) were also carried out to understand the influence of isomeric structure on the property/performance of these polymers and to explore the application of isomer chemistry in material science. Thermodynamic property and film morphology analysis of iso-P(NDI2OD-T2) and iso-P(NDI2OD-TT) were studied by thermogravimetric analysis (TGA), differential scanning calorimetry (DSC), X-ray diffraction (XRD), and atomic force microscopy (AFM). The results indicated that the films of iso-P(NDI2OD-T2) and iso-P(NDI2OD-TT) exhibited some amorphous-like features. Charge transport properties were investigated as well for these two polymers. Their top-gate bottom-contact OTFTs were fabricated by the spin-coating method using CYTOP (poly(perfluorobutenevinyl ether)) as dielectrics. Iso-P(NDI2OD-T2) exhibits mainly p-channel charge transport characteristics, with hole mobility of up to $0.3 \text{ cm}^2 \text{ V}^{-1} \text{ s}^{-1}$; this value is among the best performance of the reported disordered polymeric materials.^{27,28} Iso-P(NDI2OD-TT) displays ambipolar charge transport behaviors with electron and hole mobility of up to 4×10^{-3} and $0.020 \text{ cm}^2 \text{ V}^{-1} \text{ s}^{-1}$, respectively.

RESULTS

DFT Calculations. To gain an insight into the isomer effect on electronic structures of isomeric polymers iso-P(NDI2OD-T2)/iso-P(NDI2OD-T2) and P(NDI2OD-TT)/P(NDI2DT-TT), we carried out the molecular simulation of the trimers of these copolymers at the DFT B3LYP/6-31G* level with the Gaussian 09 package. All alkyl chains were replaced by methyl groups to reduce the time required for calculations. Figure 3 and Figure S2 show the frontier orbitals, optimized geometries, torsion angles between the NDI moieties and the adjacent donor segments, and orbital energies of the model trimers for iso-P(NDI2OD-T2)/P(NDI2OD-T2) and iso-P(NDI2OD-TT)/P(NDI2DT-TT), respectively. As shown in Figure 3, iso-P(NDI2OD-T2) and P(NDI2OD-T2) exhibit similar HOMO energy distribution, where the largest coefficients in the HOMO orbital are located along the π -conjugated polymeric backbones. A similar orbital distribution is found for iso-P(NDI2OD-TT) and P(NDI2DT-TT) (Figure S2). The results indicate that the HOMO energy distribution of NDI based D-A polymer is dominated by the donor moiety.^{17b} However, the LUMO energy distribution of these isomeric polymers are obviously different (Figure 3 and Figure S2). For polymers based on 1,2,5,6-NDI, the electron density of LUMO orbital is mainly positioned on the central NDI unit, while that of 1,4,5,8-NDI based polymers is mainly located on the three NDI segments, demonstrating that the LUMO energy distribution is mainly determined by the acceptor moiety.^{17b} The HOMO/LUMO energies of iso-P(NDI2OD-T2) estimated by DFT calculations are -5.27 and -3.12 eV, respectively, which are higher than those of P(NDI2OD-T2) (-5.46 and -3.49 eV). Similarly, the HOMO/LUMO energies of iso-P(NDI2OD-TT) (-5.52 and -3.17 eV) are also higher than those of P(NDI2DT-TT) (-5.67 and -3.59 eV). The limited electron density delocalization of LUMO energy might explain the much higher LUMO energies of iso-P(NDI2OD-T2) and iso-P(NDI2OD-TT) relative to their isomeric polymers (with a deviation of about 0.3–0.4 eV).²⁹ In addition, the weaker electron-withdrawing ability of the five-membered

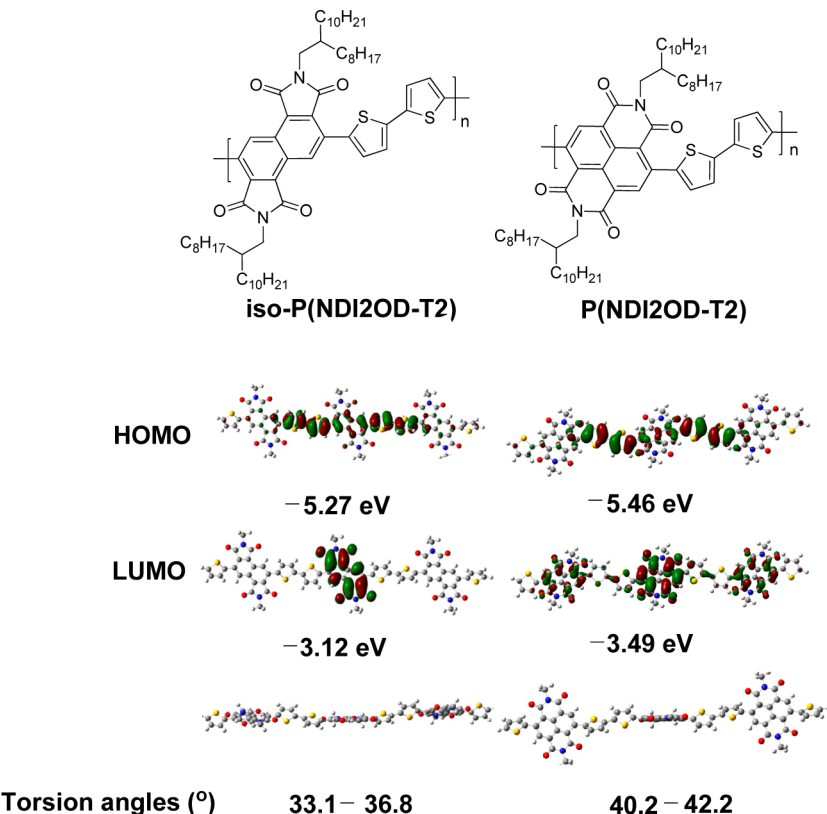
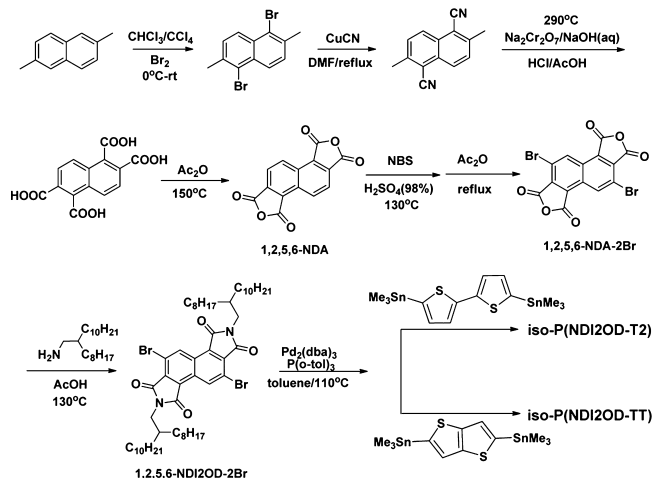


Figure 3. HOMO and LUMO orbital distributions and the minimum energy conformations of trimers of iso-P(NDI2OD-T2) and P(NDI2OD-T2) estimated by DFT calculations.

imide group relative to the six-membered one will also contribute to the higher LUMO energy. The minimum energy conformations of the model trimers show the torsion angles between the NDI moieties and the adjacent donor segments (Figure 3 and Figure S2). The 1,2,5,6-NDI based polymers have smaller torsion angles than those of 1,4,5,8-NDI based ones due to the smaller steric hindrance between the imide group and adjacent donor moiety. The DFT calculations demonstrate that the 1,2,5,6-NDI based polymers have higher HOMO/LUMO energies (especially for LUMO energy) and better planarity than those of polymers based on 1,4,5,8-NDI.

Synthesis and Characterization. The synthetic routes for copolymers iso-P(NDI2OD-T2) and iso-P(NDI2OD-TT) are shown in Scheme 1. The starting material 1,2,5,6-naphthalene dianhydride (1,2,5,6-NDA) was synthesized from the commercially available 2,6-dimethylnaphthalene according to the literature procedure.³⁰ 1,2,5,6-NDA-2Br was prepared by using NBS in 98% H₂SO₄ with a yield of 62% (the position of the bromination was demonstrated by the single crystal structure of *N,N'*-di(2-octyl)-3,7-dibromine-1,2,5,6-NDI, Figure S3). 1,2,5,6-NDA-2Br then reacted with 2-octyldodecan-1-amine in AcOH, giving 1,2,5,6-NDI2OD-2Br in 78% yield. Copolymers iso-P(NDI2OD-T2) and iso-P(NDI2OD-TT) were readily prepared via the Stille cross-coupling reaction of 1,2,5,6-NDI2OD-2Br with 5,5'-bis(trimethylstannyl)bithiophene and 2,5-bis(trimethylstannyl)thienothiophene, respectively. It is worth to note that the D/A monomer ratio of 1:1 gives the insoluble copolymer iso-P(NDI2OD-T2). After a slight change of the ratio between 1,2,5,6-NDI2OD-2Br and 5,5'-bis(trimethylstannyl)bithiophene (see Experimental Section for details), soluble iso-P(NDI2OD-T2) was obtained. Iso-P(NDI2OD-T2) and iso-P(NDI2OD-TT) were purified by

Scheme 1. Synthesis of Copolymers Iso-P(NDI2OD-T2) and Iso-P(NDI2OD-TT)



sequential Soxhlet extraction with methanol, hexane, and CHCl₃ solvents. Iso-P(NDI2OD-T2) and iso-P(NDI2OD-TT) were precipitated from the CHCl₃ fraction by the addition of methanol and characterized by ¹H NMR and elemental analysis (EA).

Molecular weights of the two polymers were determined by gel permeation chromatography (GPC) using polystyrene standards as calibrants (Figures S4 and S5). Iso-P(NDI2OD-T2) and iso-P(NDI2OD-TT) show number-average molecular weight (M_n) of 74.1 and 22.3 kDa with polydispersity indices (M_w/M_n) of 1.9 and 3.7, respectively (Table 1). Iso-P(NDI2OD-T2) has lower solubility relative to iso-P-

Table 1. Molecular Weights of the Copolymers Iso-P(NDI2OD-T2) and Iso-P(NDI2OD-TT)^a

polymer	M_n (kDa)	M_w (kDa)	M_w/M_n
iso-P(NDI2OD-T2) ^b	74.1	137.2	1.9
iso-P(NDI2OD-TT) ^b	22.3	83.3	3.7

^a M_n : number-average molecular weight; M_w : weight-average molecular weight; M_w/M_n : polydispersity index. ^bDetermined by GPC with trichlorobenzene as eluent at 150 °C on the basis of polystyrene calibration.

(NDI2OD-TT). The poor solubility of iso-P(NDI2OD-T2) is probably ascribed to the higher molecular weight (Table 1) and the stronger interchain interactions that could be explained by the better planarity of iso-P(NDI2OD-T2) versus iso-P(NDI2OD-TT), as revealed by DFT calculations (Figure 3 and Figure S2).

Optical Properties. Absorption spectra of copolymers iso-P(NDI2OD-T2) and iso-P(NDI2OD-TT) are shown in Figures 4a and 4b, respectively, where the solution spectrum was measured in dichlorobenzene and the thin films were prepared by spin-coating the dichlorobenzene solution on the quartz glass substrate. The related optical data are summarized in Table 2. As shown in Figures 4a and 4b, both iso-P(NDI2OD-T2) and iso-P(NDI2OD-TT) show a broad absorption band from 400 to 650 nm in dichlorobenzene solution with the absorption peak at 515 and 497 nm, respectively. The absorption peak of iso-P(NDI2OD-T2) exhibits a red shift both in solution (18 nm) and in film (13 nm) relative to that of iso-P(NDI2OD-TT). This might be explained by the more effective conjugation length along the polymer backbones of iso-P(NDI2OD-T2) and the stronger electron donating ability of T2 relative to TT^{17b,31} as well as the better planarity of iso-P(NDI2OD-T2) versus iso-P(NDI2OD-TT) as revealed by DFT calculations. The small red shifts of absorption peak of iso-P(NDI2OD-T2) and iso-P(NDI2OD-TT) from solution to solid state (6 and 11 nm, respectively) are in sharp contrast to the much larger red shifts of P(NDI2OD-T2) (24 nm)¹³ and P(NDI2DT-TT) (28 nm)^{17b} from solution to thin film, indicating the different π-stacking and electronic coupling for these isomeric polymers in the solid state. Thermal annealing has almost no effect on the absorption behaviors of thin films of iso-P(NDI2OD-T2) and iso-P(NDI2OD-TT) (Figure S6), indicating that films of these two iso-NDI based polymers are not sensitive to thermal treatments. Optical energy gaps (E_g^{opt}) of iso-P(NDI2OD-T2) and iso-P(NDI2OD-TT) estimated from the onset absorption of the thin films are 1.70 and 1.82 eV, respectively, which are wider than those of

P(NDI2OD-T2) and P(NDI2DT-TT) (1.50 and 1.64 eV, respectively).^{13,17b}

Electrochemical Properties. As shown in Figure 5, the oxidation and reduction potentials of iso-P(NDI2OD-T2) and iso-P(NDI2OD-TT) in thin films were determined by cyclic voltammetry (CV) in a 0.1 M Bu₄NPF₆ solution in CH₃CN (vs Ag/Ag⁺). The onset oxidation/reduction potentials of iso-P(NDI2OD-T2) and iso-P(NDI2OD-TT) are 1.10/−0.96 eV and 1.19/−1.08 eV, respectively. The HOMO/LUMO levels of iso-P(NDI2OD-T2) and iso-P(NDI2OD-TT) estimated from CV are −5.78/−3.72 eV and −5.87/−3.60 eV, respectively.

As the isomeric polymers, the HOMO energy values obtained from CV show little difference between iso-P(NDI2OD-T2) (−5.78 eV) and P(NDI2DT-T2) (−5.77 eV),^{17b} so do iso-P(NDI2OD-TT) (−5.87 eV) and P(NDI2DT-TT) (−5.80 eV),^{17b} demonstrating the donor-dominated HOMO energies. While the LUMO energies of iso-P(NDI2OD-T2) and iso-P(NDI2OD-TT) increase by about 0.19 and 0.26 eV, respectively, in comparison with those of 1,4,5,8-NDI based polymers. This might be explained by the weaker electron-deficient property of 1,2,5,6-NDI relative to that of 1,4,5,8-NDI.

Thermal Properties. Thermal stability of iso-P(NDI2OD-T2) and iso-P(NDI2OD-TT) was investigated by using thermogravimetric analysis (TGA) with a heating ramp rate of 10 °C/min under a N₂ atmosphere (Figures S7 and S8). Decomposition temperatures of iso-P(NDI2OD-T2) and iso-P(NDI2OD-TT) (at 5% weight loss) are 452 and 460 °C, respectively, demonstrating the excellent thermal stability of these two polymers. Differential scanning calorimetry (DSC) was implemented at a scan rate of 10 °C/min to investigate the phase transition of iso-P(NDI2OD-T2) and iso-P(NDI2OD-TT); no endotherm or exotherm transitions were observed from the entire scanning range of DSC (Figure S9).

Film Morphology. Morphology of the spin-coated thin films of iso-P(NDI2OD-T2) and iso-P(NDI2OD-TT) was studied by X-ray diffraction (XRD) and atom force microscopy (AFM). Figure 6 gives the XRD patterns of thin films of iso-P(NDI2OD-T2) and iso-P(NDI2OD-TT) annealed at different temperature (80, 120, 150, or 180 °C), where no obvious reflection peaks were observed even at high annealing temperature of up to 180 °C, indicating the noncrystallized nature of these two polymers. Figure 7 shows AFM images of thin films of iso-P(NDI2OD-T2) and iso-P(NDI2OD-TT) annealed at different temperature from 80 to 180 °C. For iso-P(NDI2OD-T2), the film is smooth with little self-organization within the size scales obtainable at annealing temperature of 80 °C; when annealed at 120 °C, the film exhibits some

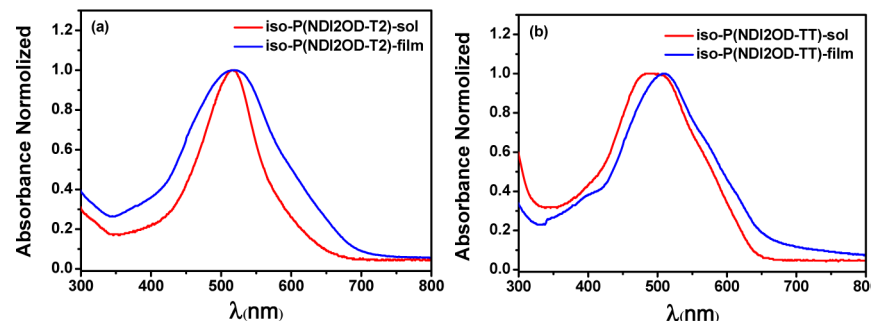


Figure 4. UV-vis absorption spectra of iso-P(NDI2OD-T2) (a) and iso-P(NDI2OD-TT) (b) in dichlorobenzene solution and thin film.

Table 2. Spectra and Electronic Energy Levels of Copolymers Iso-P(NDI2OD-T2) and Iso-P(NDI2OD-TT)

polymer	λ_{\max} soln/film (nm)	$\Delta\lambda_{\max}^a$ soln/film (nm)	E_g^{opt} (eV)	HOMO ^b (eV)	LUMO ^c (eV)	$E_g^{\text{CV}}d$ (eV)
iso-P(NDI2OD-T2)	515/521	6	1.70	-5.78	-3.72	2.06
iso-P(NDI2OD-TT)	497/508	11	1.82	-5.87	-3.60	2.27

^aThe shift of maximum absorption (λ_{\max}) from solution to film. ^bHOMO = $-(E_{\text{ox}}^{\text{onset}} - E_{1/2}(\text{Fc}/\text{Fc}^+) + 4.8)$ eV. ^cLUMO = $-(E_{\text{red}}^{\text{onset}} - E_{1/2}(\text{Fc}/\text{Fc}^+) + 4.8)$ eV. ^d E_g^{CV} = LUMO - HOMO.

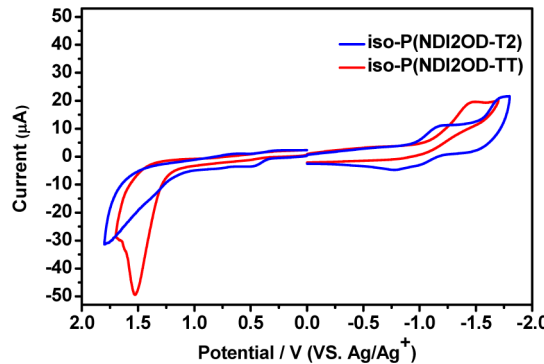


Figure 5. Cyclic voltammograms of thin films of iso-P(NDI2OD-T2) and iso-P(NDI2OD-TT) in 0.1 M $\text{Bu}_4\text{N}^+\text{PF}_6^-$ solution in acetonitrile at a scan rate of 100 mV/s.

interconnected cluster-like structures without obvious oriented crystallite domains. With the annealing temperature increasing from 150 to 180 °C, the film morphology keeps almost unchanged. The films of iso-P(NDI2OD-TT) exhibit some amorphous features without crystalline domains and film morphology variations under all thermal annealing conditions.

Field-Effect Transistors. The charge transport properties of iso-P(NDI2OD-T2) and iso-P(NDI2OD-TT) were investigated by their OTFT devices with a top-gate bottom-contact configuration (see Experimental Section for details). The influence of thermal treatments on performance of OTFTs was also studied. Figures 8 and 9 display the typical field-effect characteristics of iso-P(NDI2OD-T2) and iso-P(NDI2OD-TT), respectively. The onset annealing temperature at 80 °C is to remove the residual solvent. OTFTs based on iso-P(NDI2OD-T2) show mainly p-channel transport. By changing the annealing temperature from 80 to 180 °C, the hole mobility of iso-P(NDI2OD-T2) based OTFTs maintains in a range of $0.1\text{--}0.3 \text{ cm}^2 \text{ V}^{-1} \text{ s}^{-1}$, with current on/off ratios of $10^4\text{--}10^7$. In addition, the threshold voltages (V_T) for the p-channel mode show an increase from -19 to -36 V with the annealing temperature increasing from 80 to 180 °C, but it is unclear for this V_T increase. Interestingly, with the annealing

temperature increasing from 120 to 150 °C or even higher (180 °C), the electron transport behavior of iso-P(NDI2OD-T2) was detected with electron mobility of about $10^{-5} \text{ cm}^2 \text{ V}^{-1} \text{ s}^{-1}$ and on/off ratios of $10^3\text{--}10^4$. Iso-P(NDI2OD-TT) displays ambipolar field-effect charge transport behavior at either lower or higher annealing temperature. By elevating the annealing temperature to 180 °C, the electron mobility gains a relative high value of about $4 \times 10^{-3} \text{ cm}^2 \text{ V}^{-1} \text{ s}^{-1}$, with current on/off ratios of $10^3\text{--}10^4$, while the hole mobility mostly maintained at about $10^{-2} \text{ cm}^2 \text{ V}^{-1} \text{ s}^{-1}$, with current on/off ratios of $10^4\text{--}10^7$. The hole-dominated charge transport behavior of iso-P(NDI2OD-T2) (optimized mobility: $\mu_h = 0.3 \text{ cm}^2 \text{ V}^{-1} \text{ s}^{-1}$) and the ambipolar, hole-dominated charge transport features of iso-P(NDI2OD-TT) (optimized mobility: $\mu_h = 0.02 \text{ cm}^2 \text{ V}^{-1} \text{ s}^{-1}$; $\mu_e = 4 \times 10^{-3} \text{ cm}^2 \text{ V}^{-1} \text{ s}^{-1}$) exhibit a real difference from the electron-dominated charge transport behaviors of P(NDI2OD-T2)¹² and P(NDI2DT-TT).^{17b}

DISCUSSION

As shown in Figure 3, both iso-P(NDI2OD-T2) and iso-P(NDI2OD-TT) show well-delocalized electron density distribution of HOMO orbitals, which might yield big wave function overlap and thereby contribute to the hole transport.³² However, their limited electron density delocalization of LUMO orbitals hinder the electron transport.³² In comparison with the electron transport-dominated P(NDI2OD-T2)¹² and P(NDI2DT-TT),^{17b} the LUMO energies of iso-P(NDI2OD-T2) and iso-P(NDI2OD-TT) estimated by DFT calculations and CV results show an increase of about 0.2–0.4 eV, which increases the injection barrier of electron and goes against electron transport.

As shown in Figure S6, thermal annealing does not influence the absorption behaviors of thin films of iso-P(NDI2OD-T2) and iso-P(NDI2OD-TT); this phenomenon has also been observed in some amorphous polymers.^{28a} To further understand the microstructure of films of these two polymers, DSC, XRD, and AFM measurements were performed. No endothermic or exothermic peaks were observed from the entire scanning range of DSC (Figure S8), and no obvious reflection peaks in XRD plots were observed even at various

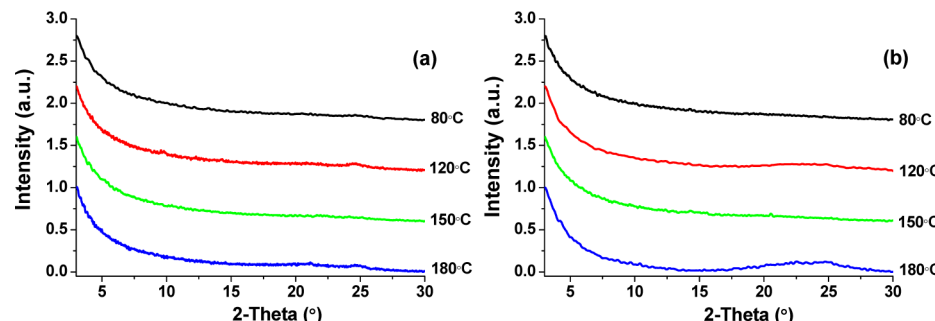


Figure 6. X-ray diffraction (XRD) patterns of spin-coated thin films of iso-P(NDI2OD-T2) (a) and iso-P(NDI2OD-TT) (b) after thermal annealing at temperatures 80, 120, 150, or 180 °C.

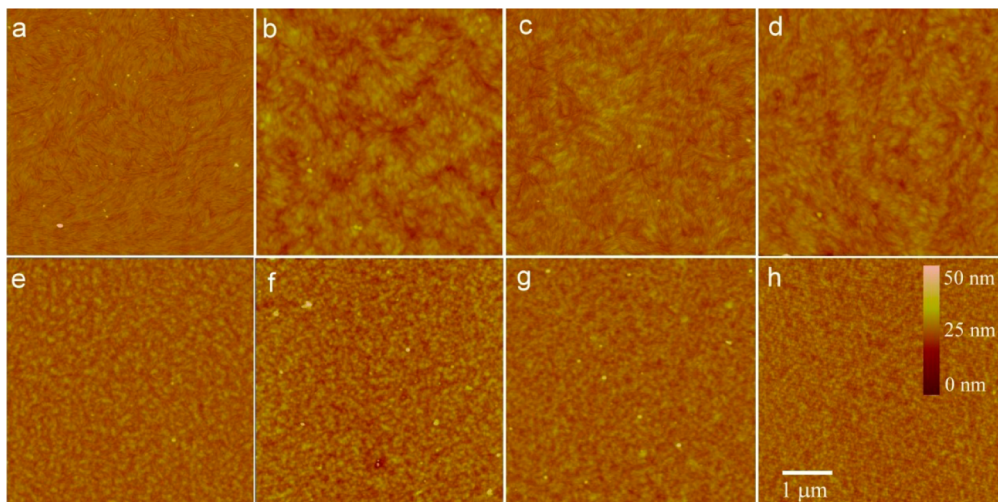


Figure 7. AFM images of thin films of iso-P(NDI2OD-T2) (a–d) and iso-P(NDI2OD-TT) (e–h) after thermal annealing at temperatures of 80 (a, e), 120 (b, f), 150 (c, g), and 180 °C (d, h), respectively.

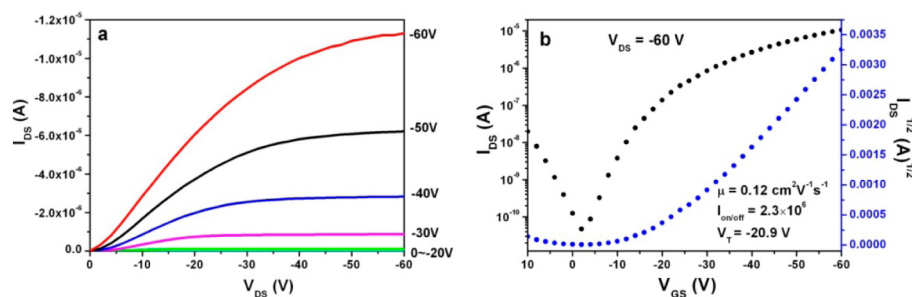


Figure 8. Output and transfer characteristics of OTFTs based on iso-P(NDI2OD-T2).

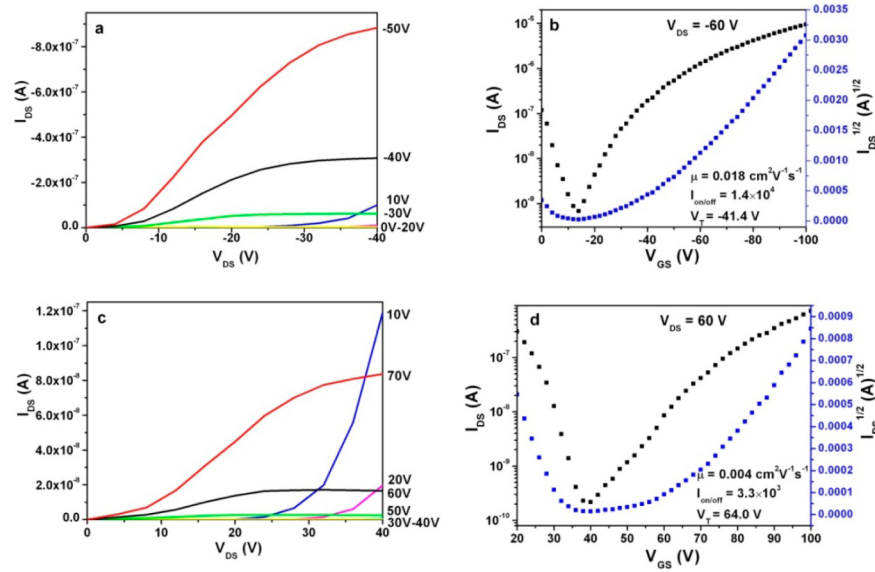


Figure 9. Output and transfer characteristics of OTFTs based on iso-P(NDI2OD-TT).

annealing temperatures (Figure 6). AFM images of thin films of iso-P(NDI2OD-T2) and iso-P(NDI2OD-TT) show few crystalline features with the annealing temperature ranging from 80 to 180 °C (Figure 7). All the results indicate that the films of iso-P(NDI2OD-T2) and iso-P(NDI2OD-TT) are amorphous-like state.²⁸

OTFT devices based on iso-P(NDI2OD-T2) and iso-P(NDI2OD-TT) exhibit different charge transport behavior from that of P(NDI2OD-T2) and P(NDI2DT-TT). Top gate OTFTs based on P(NDI2OD-T2) mainly displayed n-channel transport behavior with electron mobility of up to 0.85 cm² V⁻¹ s⁻¹.^{12a} Similar charge transport behavior of P(NDI2DT-T2) and P(NDI2DT-TT) was reported by Waston and co-

Table 3. Characteristics of OTFTs Based on Iso-P(NDI2OD-T2) and Iso-P(NDI2OD-TT) at Different Annealing Temperatures (T_a)

polymer	T_a (°C)	μ_e^a (cm ² V ⁻¹ s ⁻¹) avg (max)	V_T^a (V) avg (min)	I_{on}/I_{off}^a avg (max)	μ_h^a (cm ² V ⁻¹ s ⁻¹) avg (max)	V_T^a (V) avg (min)	I_{on}/I_{off}^a avg (max)
iso-P(NDI2OD-T2)	80				0.07 (0.11)	-18.9 (-13.6)	6×10^4 (2×10^6)
	120				0.18 (0.30)	-21.0 (-20.3)	1×10^4 (5×10^4)
	150	7×10^{-5} (7×10^{-5})	45.7 (42.8)	4×10^3 (1×10^4)	0.11 (0.26)	-29.8 (-22.2)	6×10^6 (2×10^7)
	180	3×10^{-5} (4×10^{-5})	63.5 (63.5)	2×10^4 (6×10^4)	0.08 (0.10)	-36.4 (-24.8)	2×10^5 (6×10^5)
	80	5×10^{-6} (6×10^{-6})	85.0 (85.2)	1×10^1 (2×10^1)	0.09 (0.11)	-40.9 (-37.2)	6×10^5 (2×10^6)
	120	3×10^{-6} (3×10^{-6})	80.5 (70.5)	1×10^1 (1×10^1)	0.01 (0.02)	-36.8 (-33.1)	6×10^4 (4×10^6)
iso-P(NDI2OD-TT)	150	1×10^{-6} (3×10^{-6})	83.0 (82.1)	1×10^1 (1×10^1)	0.03 (0.03)	-48.0 (-48.0)	1×10^7 (2×10^7)
	180	3×10^{-3} (4×10^{-3})	59.1 (54.2)	2×10^4 (2×10^5)	0.01 (0.02)	-31.5 (-21.6)	2×10^4 (5×10^4)

^aMobilities (μ_e/μ_h), current on/off ratios (I_{on}/I_{off}), and threshold voltages (V_T).

workers.^{17b} Either bottom-gate or top-gate OTFTs based on P(NDI2DT-T2) and P(NDI2DT-TT) mainly showed electron transport behavior; hole transport behavior could only be observed occasionally in some devices.^{17b} On the contrary, OTFTs based on iso-P(NDI2OD-T2) and iso-P(NDI2OD-TT) show hole-dominated charge transport behaviors. Top gate OTFTs based on iso-P(NDI2OD-T2) show hole mobility about $0.1\text{--}0.3$ cm² V⁻¹ s⁻¹, while the electron mobility is much lower (about 10^{-5} cm² V⁻¹ s⁻¹) and only could be measured on thin film annealed at high temperatures (150 and 180 °C). Iso-P(NDI2OD-TT) based OTFTs with the same device configuration show ambipolar charge transport behavior with average hole mobility of about 10^{-2} cm² V⁻¹ s⁻¹ and electron mobility of about $10^{-6}\text{--}10^{-5}$ cm² V⁻¹ s⁻¹ (annealing temperature: 80–150 °C). This hole-dominated charge transport behavior of iso-P(NDI2OD-T2) and iso-P(NDI2OD-TT) differs from the electron-dominated charge transport behavior of P(NDI2OD-T2) and P(NDI2OD-TT). Therefore, isomeric structure has an obvious influence on optoelectronic properties of D–A polymers, and isomer chemistry could be used as an effective strategy for fine-tuning optoelectronic properties of organic semiconducting materials.

CONCLUSION

In summary, two 1,2,5,6-NDI based D–A polymers iso-P(NDI2OD-T2) and iso-P(NDI2OD-TT) have been designed and synthesized, which could be regarded as isomeric polymers of the reported P(NDI2OD-T2) and P(NDI2DT-TT). The electronic structures, thermal, optical, and electrochemical properties were investigated and compared with those of P(NDI2OD-T2) and P(NDI2DT-TT) to investigate the influence of isomeric structure on properties of these polymers. The D–A polymers based on 1,2,5,6-NDI and 1,4,5,8-NDI exhibit a real difference in their chemical and physical properties. The UV-vis, DSC, XRD, and AFM studies all demonstrate that iso-P(NDI2OD-T2) and iso-P(NDI2OD-TT) are amorphous-like materials that are promising for flexible and large-scale optoelectronic applications. Top-gate bottom-contact OTFTs based on iso-P(NDI2OD-T2) mainly exhibit p-channel transport with hole mobility of up to 0.3 cm² V⁻¹ s⁻¹; this value is among the best performance of the disordered polymeric materials. Iso-P(NDI2OD-TT) based OTFTs show hole-dominated ambipolar field-effect characteristics with the optimized hole and electron mobility of up to 0.02 and 4×10^{-3} cm² V⁻¹ s⁻¹, respectively. The hole-dominated charge transport behavior of iso-P(NDI2OD-T2) and iso-P(NDI2OD-TT) is quite different from the electron-

dominated charge transport feature of iso-P(NDI2OD-T2) and iso-P(NDI2OD-TT). This demonstrates that isomer chemistry could be used as an effective strategy for designing new organic semiconducting materials.

EXPERIMENTAL SECTION

Materials. Chemical reagents were purchased from Aldrich or TCI and used as received. Solvents and other common reagents were obtained from the Sinopharm Chemical Reagent Co., Ltd. Toluene was distilled from sodium benzophenone ketyl under nitrogen prior to use. 1,2,5,6-NDA,³⁰ 2-octyldodecan-1-amine,^{12b} 2,2'-bithiopheneditin,^{17b} and thienothiophene-ditin^{17b} were synthesized according to the literature procedures.

Characterization. ¹H NMR spectra were measured on a Varian Mercury 300 MHz instrument using tetramethylsilane (TMS) as an internal standard. ¹³C NMR spectra were measured on a Varian Mercury 400 MHz instrument. Mass spectra (MALDI-TOF) were recorded on a Voyager-DE STR mass spectrometer. EI-MS and HRMS (MALDI) were carried out on HP5973 and InoSpec 4.7 T FT-MS, respectively. Elemental analyses were performed on an Elementar Vario EL III elemental analyzer. Electronic absorption spectra were measured on a U-3900 UV-vis spectrophotometer. TGA measurements were carried out on a TA Q500 instruments under a dry nitrogen flow at a heating rate of 10 °C/min, heating from room temperature to 500 °C. DSC analyses were performed on a TA Q2000 instrument under a nitrogen atmosphere at a heating (cooling) scan rate of 10 °C/min (rt–400 °C). Electrochemical measurements for polymers iso-P(NDI2OD-T2) and iso-P(NDI2OD-TT) were carried out on a CHI610D electrochemical workstation using a platinum working electrode coated with polymer films, a platinum-wire auxiliary electrode, and an Ag/AgNO₃ as reference electrode in a solution of tetra-n-butylammonium hexafluorophosphate (0.1 M) in CH₃CN at a scan rate of 100 mV/s. The gel permeation chromatography (GPC) measurements were performed on PL-GPC220 instrument at 150 °C, using trichlorobenzene as eluent and polystyrene standards as calibrants. AFM was recorded on a Nanoscope IIIa atomic force microscopy (AFM) in tapping mode.

Fabrication of Top Gate Bottom Contact OTFTs. Borosilicate glass was used as the substrate for all the top gate devices after cleaning in an ultrasonic bath with deionized water, ethanol, and acetone. The gold source-drain electrodes were patterned by a typical photolithography process. All the substrates were treated with octadecyltrichlorosilane (OTS) at 120 °C for 3 h in a vacuum oven. The organic active layer was deposited by a spin-coating process (7 mg/mL in dichlorobenzene) under atmosphere. Then the films were annealed at different temperatures (80, 120, 150, or 180 °C) for 1 h under vacuum, and the cooling rate for the XRD, AFM, and OTFTs experiment is 1.5 °C/min. The perfluorinated polymer CYTOP (CTL-809M) was spun at 2000 rpm for 60 s as the dielectric. Finally, 40 nm Al was thermally evaporated as the gate electrodes. The FET properties were calculated in the saturation regime.

Synthesis. 1,2,5,6-NDA. In a 250 mL stainless steel autoclave, 2.1 g of 1,5-dicyano-2,6-dimethylnaphthalene was added to 40 mL of aqueous solution containing $\text{Na}_2\text{Cr}_2\text{O}_7 \cdot 2\text{H}_2\text{O}$ (10.1 g). The mixture was sealed and stirred at 290 °C for 6 h. After the mixture was cooled and filtered, the basic solution was treated with ether. Crude 1,2,5,6-naphthalenetetracarboxylic acid was reprecipitated from water by adding hydrochloric acid. Yellow precipitate was collected and refluxed in AcOH for 3 h, and then the solid was collected by filtration and applied to next reaction without further purification. The obtained 2.47 g crude product was refluxed in 120 mL of acetic anhydride for 3 h, and 1.9 g yellowish white product was obtained by filtration (yield: 75%). MS (EI) m/z : 268 (M^+); Anal. Calcd for $\text{C}_{14}\text{H}_4\text{O}_6$: C, 62.70; H, 1.50. Found: C, 62.50; H, 1.63.

1,2,5,6-NDA-2Br. 1,2,5,6-NDA (200 mg, 0.66 mmol) and NBS (585 mg, 3.29 mmol) were dissolved in 10 mL of H_2SO_4 (98%) and stirred at 130 °C for 24 h in a dark environment. When the mixture was cooled to room temperature, it was poured into ice water. The solution was extracted by ethyl acetate. When the combined ethyl acetate solution was removed under reduced pressure, a yellow solid was obtained. Then, the yellow solid was dissolved in acetic anhydride and refluxed for 5 h. When the reaction mixture was cooled to room temperature, it was filtered, and 175 mg of deep green solid was obtained. The crude product was used without further purification (yield: 62%). MS (EI) m/z : 426 (M^+); HRMS (EI): 423.8222 (calc mass: 423.8218).

1,2,5,6-NDI2OD-2Br. 1,2,5,6-NDA-2Br (200 mg, 0.47 mmol) was reacted with 2-octyldodecan-1-amine (322 mg, 1.08 mmol) in refluxed glacial acetic acid for 3 h. The reaction mixture was then cooled to room temperature. After removing the acetic acid under reduced pressure, the crude product was purified by column chromatography, using the mixture of petroleum ether and dichloromethane (2:1) as the eluent. 360 mg of yellow product was obtained (yield: 78%). ^1H NMR (300 MHz, CDCl_3) δ (ppm): 0.84–0.87 (t, 12H), 1.23 (m, 64H), 1.90 (br, 2H, CH), 3.62–3.63 (m, 4H), 9.50 (S, 2H). ^{13}C NMR (100 MHz, CDCl_3): δ 14.09, 22.66, 26.31, 29.27, 29.32, 29.52, 29.61, 29.90, 31.52, 31.69, 31.88, 31.89, 43.88, 98.72, 117.24, 128.10, 130.07, 130.78, 135.84, 166.00, 167.27. MS (MALDI-TOF) m/z : 986.2 ($\text{M} + \text{H}^+$); Anal. Calcd for $\text{C}_{35}\text{H}_{49}\text{N}_3\text{O}_3\text{S}_2$: C, 65.84; H, 8.60; N, 2.84. Found: C, 65.80; H, 8.56; N, 2.79.

Diocetyl-1,2,5,6-NDI-2Br. Diocetyl-1,2,5,6-NDI-2Br was synthesized following the same procedure as 1,2,5,6-NDI2OD-2Br. Diocetyl-1,2,5,6-NDI-2Br was obtained as yellow solid (yields: 56%). ^1H NMR (300 MHz, CDCl_3) δ (ppm): 0.85–0.89 (t, 6H), 1.27–1.34 (m, 20H), 1.70–1.75 (br, 4H), 3.73–3.78 (t, 4H), 9.53 (s, 2H). MS (MALDI-TOF) m/z : 649 ($\text{M} + \text{H}^+$). Anal. Calcd for $\text{C}_{30}\text{H}_{38}\text{N}_2\text{O}_4$: C, 55.57; H, 5.60; N, 4.32. Found: C, 55.65; H, 5.45; N, 4.12.

Iso-P(NDI2OD-T2). To a mixture of 1,2,5,6-NDI2OD-2Br (180 mg, 0.183 mmol) and 5,5'-bis(trimethylstannyl)bithiophene (88 mg, 0.179 mmol) in toluene (20 mL) was added $\text{Pd}_2(\text{dba})_3$ (3.5 mg, 2% mmol) and $\text{P}(\text{o-tol})_3$ (4.5 mg, 8% mmol) under a N_2 atmosphere. The mixture was stirred at 110 °C for 24 h. After the reaction mixture was cooled to room temperature, chloroform (100 mL) was added, and the mixture was washed with water. The organic phase was concentrated to 10 mL and dropped into methanol (500 mL). A green precipitate was filtered. The resulting solid was subjected to Soxhlet extraction successively with methanol, acetone, and hexane to remove the oligomers and impurities. The remaining polymer was extracted with chloroform and precipitated again from methanol, filtered, washed with methanol, and dried under vacuum. 170 mg of dark-green copolymer was obtained (yield: 94%). ^1H NMR (300 MHz, $\text{C}_6\text{D}_4\text{Cl}_2$) δ (ppm): 0.93–3.00 (br, 78H), 4.00 (br, 4H) 7.45–9.60 (br, 6H). Anal. Calcd for $\text{C}_{35}\text{H}_{49}\text{N}_3\text{O}_3\text{S}_2$: C, 75.10; H, 9.15; N, 2.83. Found: C, 75.10; H, 8.83; N, 2.73.

Iso-P(NDI2OD-TT). To a mixture of 1,2,5,6-NDI2OD-2Br (200 mg, 0.203 mmol) and 2,5-bis(trimethylstannyl)thienothiophene (95 mg, 0.203 mmol) in toluene (20 mL) was added $\text{Pd}_2(\text{dba})_3$ (3.7 mg, 2% mmol) and $\text{P}(\text{o-tol})_3$ (4.9 mg, 8% mmol) under a N_2 atmosphere. The mixture was stirred at 110 °C for 42 h. After the reaction mixture was cooled to room temperature, chloroform (100 mL) was added, and the mixture was washed with water. The organic phase was

concentrated to 10 mL and dropped into methanol (500 mL). A green precipitate was filtered. The resulting solid was subjected to Soxhlet extraction successively with methanol, acetone, and hexane to remove the oligomers and impurities. The remaining polymer was extracted with chloroform and precipitated again from methanol, filtered, washed with methanol, and dried under vacuum. 190 mg dark-green of copolymer was obtained (yield: 97%). ^1H NMR (300 MHz, CDCl_3) δ (ppm): 0.82–3.72 (br, 82H), 8.01–9.40 (br, 4H). Anal. Calcd for $\text{C}_{35}\text{H}_{49}\text{N}_3\text{O}_3\text{S}_2$: C, 74.64; H, 9.19; N, 2.90. Found: C, 74.46; H, 8.82; N, 2.80.

ASSOCIATED CONTENT

Supporting Information

DFT calculations, UV-vis spectra, TGA/DSC plots, MS, GPC, and NMR spectra of iso-P(NDI2OD-T2), iso-P(NDI2OD-TT), or the related compounds. This material is available free of charge via the Internet at <http://pubs.acs.org>.

AUTHOR INFORMATION

Corresponding Authors

*E-mail gaoxk@mail.sioc.ac.cn (X.G.).

*E-mail dicha@iccas.ac.cn (C.D.).

Notes

The authors declare no competing financial interest.

ACKNOWLEDGMENTS

The present research was financially supported by National Natural Science Foundation (51173200, 61171055, and 21103023), MOST (2211CB932300), and the Chinese Academy of Sciences.

REFERENCES

- (a) Gelinck, G. H.; Geuns, T. C. T.; de Leeuw, D. M. *Appl. Phys. Lett.* **2000**, 77, 1487–1489. (b) Huitema, H. E. A.; et al. *Nature* **2001**, 414, 599. (c) Arias, A. C.; MacKenzie, J. D.; McCulloch, I.; Rivnay, J.; Salleo, A. *Chem. Rev.* **2010**, 110, 3–24. (d) Rogers, J. A.; Someya, T.; Huang, Y. G. *Science* **2010**, 327, 1603–1607. (e) Gelinck, G.; Heremans, P.; Nomoto, K.; Anthopoulos, T. D. *Adv. Mater.* **2010**, 22, 3778–3798.
- (a) Marks, T. J. *MRS Bull.* **2010**, 35, 1018. (b) Facchetti, A. *Chem. Mater.* **2011**, 23, 733–758.
- (3) Liu, J. Y.; Zhang, R.; Sauve, G.; Kowalewski, T.; McCullough, R. D. *J. Am. Chem. Soc.* **2008**, 130, 13167–13176.
- (4) (a) Bao, Z.; Dodabalapur, A.; Lovinger, A. J. *Appl. Phys. Lett.* **1996**, 69, 4108–4110. (b) Sirringhaus, H.; Tessler, N.; Friend, R. H. *Science* **1998**, 280, 1741–1744. (c) Sirringhaus, H.; Brown, P. J.; Friend, R. H.; Nielsen, M. M.; Bechgaard, K.; Langeveld-Voss, B. M. W.; Spiering, A. J. H.; Janssen, R. A. J.; Meijer, E. W.; Herwig, P.; de Leeuw, D. M. *Nature* **1999**, 401, 685–688. (d) Wang, G. M.; Swensen, J.; Moses, D.; Heeger, A. J. *J. Appl. Phys.* **2003**, 93, 6137–6141.
- (5) (a) Lim, E.; Jung, B. J.; Lee, J.; Shim, H. K.; Lee, J. I.; Yang, Y. S.; Do, L. M. *Macromolecules* **2005**, 38, 4531–4535. (b) McCulloch, I.; Heeney, M.; Bailey, C.; Genevicius, K.; I, M.; Shkunov, M.; Sparrowe, D.; Tierney, S.; Wagner, R.; Zhang, W. M.; Chabinyc, M. L.; Kline, R. J.; McGehee, M. D.; Toney, M. F. *Nat. Mater.* **2006**, 5, 328–333. (c) Li, Y. N.; Wu, Y. L.; Liu, P.; Birau, M.; Pan, H. L.; Ong, B. S. *Adv. Mater.* **2006**, 18, 3029–3032. (d) He, M. Q.; Li, J. F.; Sorensen, M. L.; Zhang, F. X.; Hancock, R. R.; Fong, H. H.; Pozdin, V. A.; Smilgies, D. M.; Malliaras, G. G. *J. Am. Chem. Soc.* **2009**, 131, 11930–11938. (e) Rieger, R.; Beckmann, D.; Pisula, W.; Steffen, W.; Kastler, M.; Mullen, K. *Adv. Mater.* **2010**, 22, 83–86.
- (6) (a) Agrawal, A. K.; Jenekhe, S. A. *Macromolecules* **1991**, 24, 6806–6808. (b) Jenekhe, S. A.; Lu, L. D.; Alam, M. M. *Macromolecules* **2001**, 34, 7315–7324. (c) van Mullekom, H. A. M.; Vekemans, J. A. J. M.; Havinga, E. E.; Meijer, E. W. *Mater. Sci. Eng., R* **2001**, 32, 1–40.

- (d) Kroon, R.; Lenes, M.; Hummelen, J. C.; Blom, P. W. M.; De Boer, B. *Polym. Rev.* **2008**, *48*, 531–582.
- (7) (a) Tsao, H. N.; Cho, D. M.; Park, I.; Hansen, M. R.; Mavrinskiy, A.; Yoon, D. Y.; Graf, R.; Pisula, W.; Spiess, H. W.; Mullen, K. *J. Am. Chem. Soc.* **2011**, *133*, 2605–2612. (b) Lei, T.; Cao, Y.; Fan, Y.; Liu, C.-J.; Yuan, S.-C.; Pei, J. *J. Am. Chem. Soc.* **2011**, *133*, 6099–6101. (c) Zhang, X.; Richter, L. J.; DeLongchamp, D. M.; Kline, R. J.; Hammond, M. R.; McCulloch, I.; Heeney, M.; Ashraf, R. S.; Smith, J. N.; Anthopoulos, T. D.; Schroeder, B.; Geerts, Y. H.; Fischer, D. A.; Toney, M. F. *J. Am. Chem. Soc.* **2011**, *133*, 15073–15084.
- (8) (a) Beaujuge, P. M.; Amb, C. M.; Reynolds, J. R. *Acc. Chem. Res.* **2010**, *43*, 1396–1407. (b) Cheng, Y. J.; Yang, S. H.; Hsu, C. S. *Chem. Rev.* **2009**, *109*, 5868–5923.
- (9) (a) Biniek, L.; Schroeder, B. C.; Nielsen, C. B.; McCulloch, I. J. *Mater. Chem.* **2012**, *22*, 14803–14813. (b) Boudreault, P. L. T.; Najari, A.; Leclerc, M. *Chem. Mater.* **2011**, *23*, 456–469.
- (10) Guo, X. G.; Watson, M. D. *Macromolecules* **2011**, *44*, 6711–6716.
- (11) (a) Zhan, X. W.; Tan, Z. A.; Domercq, B.; An, Z. S.; Zhang, X.; Barlow, S.; Li, Y. F.; Zhu, D. B.; Kippelen, B.; Marder, S. R. *J. Am. Chem. Soc.* **2007**, *129*, 7246–7247. (b) Tan, Z. A.; Zhou, E. J.; Zhan, X. W.; Wang, X.; Li, Y. F.; Barlow, S.; Marder, S. R. *Appl. Phys. Lett.* **2008**, *93*, 073309. (c) Zhan, X. W.; Tan, Z. A.; Zhou, E. J.; Li, Y. F.; Misra, R.; Grant, A.; Domercq, B.; Zhang, X. H.; An, Z. S.; Zhang, X.; Barlow, S.; Kippelen, B.; Marder, S. R. *J. Mater. Chem.* **2009**, *19*, 5794–5803. (d) Zhou, E.; Tajima, K.; Yang, C. H.; Hashimoto, K. *J. Mater. Chem.* **2010**, *20*, 2362–2368. (e) Huang, J.; Wu, Y.; Fu, H. B.; Zhan, X. W.; Yao, J. N.; Barlow, S.; Marder, S. R. *J. Phys. Chem. A* **2009**, *113*, 5039–5046. (f) Zhao, X.; Ma, L.; Zhang, L.; Wen, Y.; Chen, J.; Shuai, Z.; Liu, Y.; Zhan, X. *Macromolecules* **2013**, *46*, 2152–2158.
- (12) (a) Yan, H.; Chen, Z. H.; Zheng, Y.; Newman, C.; Quinn, J. R.; Dotz, F.; Kastler, M.; Facchetti, A. *Nature* **2009**, *457*, 679. (b) Chen, Z. H.; Zheng, Y.; Yan, H.; Facchetti, A. *J. Am. Chem. Soc.* **2009**, *131*, 8–9.
- (13) Durban, M. M.; Kazarinoff, P. D.; Luscombe, C. K. *Macromolecules* **2010**, *43*, 6348–6352.
- (14) Zhan, X. W.; Facchetti, A.; Barlow, S.; Marks, T. J.; Ratner, M. A.; Wasielewski, M. R.; Marder, S. R. *Adv. Mater.* **2011**, *23*, 268–284.
- (15) (a) Hu, Y. B.; Gao, X. K.; Di, C. A.; Yang, X. D.; Zhang, F.; Liu, Y. Q.; Li, H. X.; Zhu, D. B. *Chem. Mater.* **2011**, *23*, 1204–1215. (b) Zhang, F.; Hu, Y.; Schuettfort, T.; Di, C.-a.; Gao, X.; McNeill, C. R.; Thomsen, L.; Mannsfeld, S. C. B.; Yuan, W.; Sirringhaus, H.; Zhu, D. *J. Am. Chem. Soc.* **2013**, *135*, 2338–2349.
- (16) (a) Babel, A.; Jenekhe, S. A. *Adv. Mater.* **2002**, *14*, 371–374. (b) Babel, A.; Jenekhe, S. A. *J. Am. Chem. Soc.* **2003**, *125*, 13656–13657. (c) Briseno, A. L.; Kim, F. S.; Babel, A.; Xia, Y. N.; Jenekhe, S. A. *J. Mater. Chem.* **2011**, *21*, 16461–16466.
- (17) (a) Kim, F. S.; Guo, X.; Watson, M. D.; Jenekhe, S. A. *Adv. Mater.* **2010**, *22*, 478–482. (b) Guo, X. G.; Kim, F. S.; Seger, M. J.; Jenekhe, S. A.; Watson, M. D. *Chem. Mater.* **2012**, *24*, 1434–1442.
- (18) (a) Ahmed, E.; Ren, G. Q.; Kim, F. S.; Hollenbeck, E. C.; Jenekhe, S. A. *Chem. Mater.* **2011**, *23*, 4563–4577. (b) Ren, G. Q.; Ahmed, E.; Jenekhe, S. A. *Adv. Energy Mater.* **2011**, *1*, 946–953. (c) Ren, G. Q.; Ahmed, E.; Jenekhe, S. A. *J. Mater. Chem.* **2012**, *22*, 24373–24379.
- (19) (a) Kolhe, N. B.; Asha, S. K.; Senanayak, S. P.; Narayan, K. S. *J. Phys. Chem. B* **2010**, *114*, 16694–16704. (b) Hwang, Y. J.; Ren, G. Q.; Murari, N. M.; Jenekhe, S. A. *Macromolecules* **2012**, *45*, 9056–9062. (c) Popere, B. C.; Della Pelle, A. M.; Thayumanavan, S. *Macromolecules* **2011**, *44*, 4767–4776. (d) Durban, M. M.; Kazarinoff, P. D.; Segawa, Y.; Luscombe, C. K. *Macromolecules* **2011**, *44*, 4721–4728. (e) Zhou, W. Y.; Wen, Y. G.; Ma, L. C.; Liu, Y. Q.; Zhan, X. W. *Macromolecules* **2012**, *45*, 4115–4121.
- (20) (a) Meng, Q.; Hu, W. P. *Phys. Chem. Chem. Phys.* **2012**, *14*, 14152–14164. (b) Bhosale, S. V.; Bhosale, S. V.; Bhargava, S. K. *Org. Biomol. Chem.* **2012**, *10*, 6455.
- (21) (a) Shinamura, S.; Osaka, I.; Miyazaki, E.; Nakao, A.; Yamagishi, M.; Takeya, J.; Takimiya, K. *J. Am. Chem. Soc.* **2011**, *133*, 5024–5035. (b) Mas-Montoya, M.; Ortiz, R. P.; Curiel, D.; Espinosa, A.; Allain, M.; Facchetti, A.; Marks, T. J. *J. Mater. Chem. C* **2013**, *1*, 1959–1969.
- (22) (a) Okamoto, H.; Kawasaki, N.; Kaji, Y.; Kubozono, Y.; Fujiwara, A.; Yamaji, M. *J. Am. Chem. Soc.* **2008**, *130*, 10470. (b) Bendikov, M.; Wudl, F.; Perepichka, D. F. *Chem. Rev.* **2004**, *104*, 4891–4945.
- (23) (a) Osaka, I.; Abe, T.; Shinamura, S.; Takimiya, K. *J. Am. Chem. Soc.* **2011**, *133*, 6852–6860. (b) Rieger, R.; Beckmann, D.; Mavrinskiy, A.; Kastler, M.; Mullen, K. *Chem. Mater.* **2010**, *22*, 5314–5318. (c) Facchetti, A.; Yoon, M. H.; Stern, C. L.; Katz, H. E.; Marks, T. J. *Angew. Chem., Int. Ed.* **2003**, *42*, 3900–3903. (d) Huang, Y.; Zhang, M. Q.; Ye, L.; Guo, X.; Han, C. C.; Li, Y. F.; Hou, J. H. *J. Mater. Chem.* **2012**, *22*, 5700–5705. (e) Li, S.; He, Z. C.; Yu, J.; Chen, S. A.; Zhong, A. S.; Tang, R. L.; Wu, H. B.; Qin, J. G.; Li, Z. *J. Mater. Chem.* **2012**, *22*, 12523–12531.
- (24) Bhosale, S. V.; Jani, C. H.; Langford, S. *J. Chem. Soc. Rev.* **2008**, *37*, 331–342.
- (25) Chen, S. C.; Zhang, Q. K.; Zheng, Q. D.; Tang, C. Q.; Lu, C. Z. *Chem. Commun.* **2012**, *48*, 1254–1256.
- (26) During the preparation of this work, a similar D–A copolymer based on 1,2,5,6-NDI and 2,2'-bithiophene was reported by Zheng's group: Chen, S. C.; Zheng, Q. D.; Zhang, Q. K.; Cai, D. D.; Wang, J. Y.; Y, Z. G.; Tang, C. Q. *J. Polym. Sci., Part A: Polym. Chem.* **2013**, *51*, 1999–2005.
- (27) Tsao, H. N.; Mullen, K. *Chem. Soc. Rev.* **2010**, *39*, 2372–2386.
- (28) (a) Chung, D. S.; Lee, S. J.; Park, J. W.; Choi, D. B.; Lee, D. H.; Park, J. W.; Shin, S. C.; Kim, Y. H.; Kwon, S. K.; Park, C. E. *Chem. Mater.* **2008**, *20*, 3450–3456. (b) Baek, N. S.; Hau, S. K.; Yip, H. L.; Acton, O.; Chen, K. S.; Jen, A. K. Y. *Chem. Mater.* **2008**, *20*, 5734–5736. (c) Lee, J.; Cho, S.; Yang, C. *J. Mater. Chem.* **2011**, *21*, 8528–8531.
- (29) (a) Lee, S. J.; Park, J. S.; Yoon, K. J.; Kim, Y. I.; Jin, S. H.; Kang, S. K.; Gal, Y. S.; Kang, S.; Lee, J. Y.; Kang, J. W.; Lee, S. H.; Park, H. D.; Kim, J. J. *Adv. Funct. Mater.* **2008**, *18*, 3922–3930. (b) Zhang, H. Q.; Wan, X. J.; Xue, X. S.; Li, Y. Q.; Yu, A.; Chen, Y. S. *Eur. J. Org. Chem.* **2010**, 1681–1687.
- (30) Sato, T.; Niino, H.; Yabe, A. *Chem. Commun.* **2000**, 1205–1206.
- (31) Tang, W.; Ke, L.; Tan, L.; Lin, T.; Kietzke, T.; Chen, Z.-K. *Macromolecules* **2007**, *40*, 6164–6171.
- (32) Coropceanu, V.; Cornil, J.; da Silva, D. A.; Olivier, Y.; Silbey, R.; Bredas, J. L. *Chem. Rev.* **2007**, *107*, 2165–2165.